Geochemical Perspectives Letters

Published by the European Association of Geochemistry

Imaging of boron in altered mantle rocks illuminates progressive serpentinisation episodes

A.D. Evans[1*], C.D. Standish[1], J.A. Milton[1], A.G. Robbins[1], D. Craw[2], G.L. Foster[1], D.A.H. Teagle[1]

Abstract

https://doi.org/10.7185/geochemlet.2407

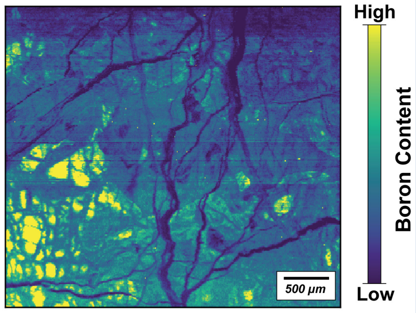

Serpentinised mantle rocks reflect the cumulative sum of multiple alteration events, but to date, identifying distinct serpentinisation episodes has remained challenging due to limited knowledge of the spatial distribution of tracers of fluid-rock exchange. Here we present novel high spatial resolution (~10 µm) boron, nickel, calcium, and lithium concentration maps combined with *in situ* boron isotope analyses of strongly serpentinised mantle peridotites from the Troodos ophiolite, Cyprus. Our maps indicate strongly heterogenous boron concentrations with high boron concentrations in early formed serpentine replacing olivine but much lower boron contents in mesh-textured serpentine and bastitic pyroxene. Late stage crosscutting serpentine veins have very low boron concentrations. In contrast, boron isotope measurements, made at coarser scales, are remarkably uniform (mean value +11.9 ± 3.2 ‰, 1σ, n = 49). We interpret the high boron serpentine as reflecting the partial preservation of an early pervasive serpentinisation episode by fluids with high boron concentrations sourced from the dehydration of the subducting Cyprus slab. Subsequent serpentine phases with moderate to low boron reflect progressive recrystallisation and leaching by low boron concentration meteoric waters.

Received 3 July 2023 | Accepted 22 January 2024 | Published 23 February 2024

Introduction

Serpentinisation, the interaction of water with mantle rocks, is a crucial process in the Earth system, influencing the planetary water cycle. It plays a key role in plate tectonics (Guillot *et al.*, 2015), forms mountains through isostatic uplift (Evans *et al.*, 2021), and stores water, carbon, and fluid-mobile elements (Kodolányi *et al.*, 2012). Understanding where, when, and with what fluids mantle rock alteration occurs is vital for quantifying serpentinisation's role in planetary cycles. Existing evidence, such as crosscutting relationships and stable isotopic compositions, suggests a progressive series of reactions during multiple water-rock interaction episodes (Alt and Shanks, 2006). However, determining the conditions of distinct serpentinisation events is challenging due to the complex geological histories of altered mantle rocks, often overwritten by subsequent interactions (Kyser and Kerrich, 1991). Whole rock analyses reflect cumulative signatures, making geochemical and isotopic fingerprinting of discrete events difficult (Wenner and Taylor, 1973; Alt and Shanks, 2006) due to poorly constrained spatial and temporal distributions of elemental and isotopic changes resulting from serpentinisation events.

Boron, an abundant element in serpentine with concentrations reaching ~250 µg/g (Pabst *et al.*, 2011), far exceeds levels in the primitive mantle (<0.25 µg/g; Marschall *et al.*, 2017). This discrepancy makes boron and its isotopes valuable for discerning serpentinisation processes and conditions (Boschi *et al.*, 2008; Vils *et al.* 2009; Martin *et al.*, 2016). Previous studies noted variations in boron concentrations and isotopic compositions, yet the lack of spatial context raises uncertainty about whether these variations indicate distinct serpentinisation events or the accumulation of successive episodes.

Our investigation focuses on the Troodos ophiolite's serpentinised mantle rocks, utilising high resolution (10 µm/pixel) 2D maps of boron content, calibrated against *in situ* and powder measurements. In conjunction with *in situ* boron isotope analyses, our results reveal contrasting boron signatures in the strongly altered Troodos mantle peridotites. This allows us to identify distinct serpentinisation events by contrasting fluid sources.

Geological Setting

The Troodos Massif in Cyprus houses an exceptionally well preserved ophiolite sequence, featuring an elliptical bullseye-patterned welt at its centre (Fig. 1a). This welt, with the highest elevations composed of mantle peridotites, is part of the Troodos Mantle Sequence, which is divided into two regions: the Olympus and Artemis domains (Wilson, 1959) that are interpreted as nested serpentinite diapirs with contrasting serpentinisation and deformation styles and intensities (Evans *et al.*, 2021).

---

1. School of Ocean and Earth Science, National Oceanography Centre Southampton, University of Southampton, European Way, Southampton, SO14 3ZH, UK
2. Department of Geology, University of Otago, P.O. Box 56, Dunedin, New Zealand
* Corresponding author (email: a.evans@soton.ac.uk)

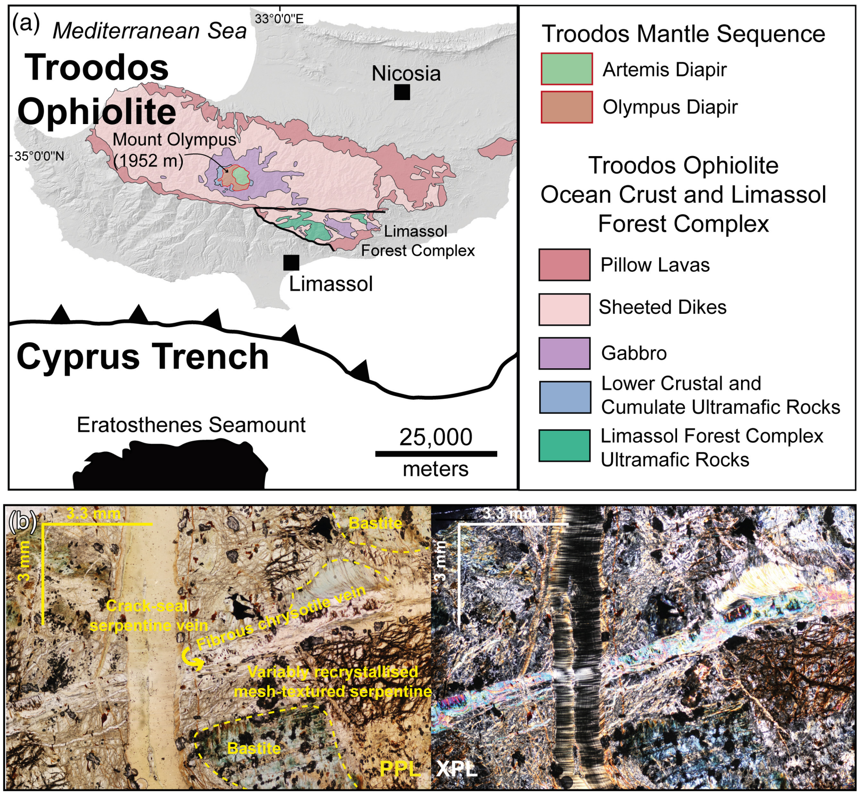

Figure 1 **(a)** Geological map of the Troodos ophiolite with the bullseye geometry of the Mantle Sequence highlighted (adapted from Evans *et al*., 2021). **(b)** Representative photomicrograph of completely serpentinised mantle peridotite located within the Artemis Diapir with variably recrystallised serpentine mesh texture, bastite, crack-seal serpentine vein and fibrous chrysotile vein. Scale bar is proportional to the mapped region of Figure 2.

The Olympus Diapir consists of partially serpentinised tectonised harzburgites, while the Artemis Diapir is a sub-circular region with completely serpentinised peridotite blocks and clasts in a serpentinite breccia matrix (Wilson, 1959; Evans *et al.*, 2021). The Artemis rocks display variably recrystallised mesh-textured serpentine assemblages with distinctive features, including mutually crosscutting, fibrous asbestiform chrysotile and crack-seal serpentine vein sets (Fig. 1b). These serpentinite diapirs are proposed to originate from the tectonic juxtaposition of geochemically distinct mantle regions through serpentinite diapirism (Batanova and Sobolev, 2000).

The Troodos ophiolite originated at a Neo-Tethyan spreading ridge around 90–92 million years ago above a supra-subduction zone (Moores *et al.*, 1984). However, its recent uplift and exposure, approximately 5.5 million years ago, is attributed to concentrated serpentinisation of the mantle wedge above a new north-dipping subduction zone. This zone consumes old oceanic crust, at least Mesozoic in age, on the leading edge of the Sinai plate (Cyprus slab) in the Cyprean trench to the south of the island. The initiation of subduction occurred in the early Miocene (~20 million years ago) (Robertson, 1998; Feld *et al.*, 2017). A significant negative Bouguer anomaly is centred on the Artemis Diapir, modelled as a vertical, cylindrical body of low density (~2,700 kg/m^3) strongly serpentinised peridotite extending to a depth of approximately 11 km. This depth aligns with the inferred minimum depth of the top of the downgoing plate (Gass and Masson-Smith, 1963; Feld *et al.*, 2017). It's important to note that modern subduction differs from the supra-subduction zone setting that led to the formation of the Troodos ophiolite (Moores *et al.*, 1984; Robertson, 1998). Subduction beneath Cyprus stalled due to the collision of the Eratosthenes plateau with the Cyprean trench less than 5 million years ago. This collision focused fluids released by the dehydration of the downgoing Cyprus slab beneath the Mount Olympus region, inducing serpentinisation hydration reactions and isostatic uplift (Robertson, 1998; Evans *et al.*, 2021, 2024).

The Troodos mantle peridotites have been uplifted and exposed since the Pleistocene (Poole and Robertson, 1991), a process enhanced by the incursion of meteoric waters. Oxygen and hydrogen isotope analyses of serpentinised Troodos rocks have yielded various interpretations, including exchange with Cretaceous seawater at the spreading ridge, exchange at 200 to 300 °C with waters sourced from the Cyprus slab, or exchange at less than 50 °C with meteoric water (Magaritz and Taylor, 1974; Sheppard, 1980; Nuriel *et al.*, 2009; Evans *et al.*, 2021, 2024).

Analytical Methods

Boron concentrations were mapped in polished serpentinite thick sections using a 10 × 10 µm ablation beam from an Elemental Scientific Lasers NWR193 Excimer laser ablation (LA) system with a TwoVol2 ablation cell coupled to an Agilent 8900 Triple Quadrupole ICP-MS. Boron concentrations were calibrated against *in situ* and pressed powder pellet (PPP) boron concentrations determined at coarser resolutions (150 × 50 µm). Boron isotope analyses of polished thick sections and pressed powder pellets (PPP) were acquired using a Thermo Scientific Neptune Plus multi-collector inductively coupled plasma (MC-ICP) mass spectrometer. For more details on our analytical procedures refer to the Supplementary Information.

Results

The *in situ* boron elemental 2D map of a fully serpentinised sample from the Artemis Diapir (Fig. 2a) indicates three distinct serpentine styles with varying boron concentrations: 1) high boron concentration serpentine, pseudomorphing original olivine grains, 2) moderate boron serpentine, coexisting with the B-rich style, and 3) discrete, irregular low boron concentration serpentine veins and mesh-textured background serpentine, which crosscuts types 1 and 2. The nickel content map (Fig. 2b) reflects the original primary texture before serpentinisation, with former olivine grains exhibiting high nickel contents and former pyroxene grains having relatively lower nickel contents. Calcium maps (Fig. 2c) highlight the contrast between mesh-textured serpentine and serpentine veins, with high calcium counts indicating calcium-rich inclusions. Lithium contents (Fig. 2d) show a distinct pattern from boron, with high lithium content occurring in serpentine pseudomorphing original pyroxene grains, while some late stage serpentine veins with mesh-textured serpentine generally have low lithium contents.

Samples from the Olympus and Artemis diapirs show similar boron concentrations and isotopic compositions (Fig. 3). In the Troodos Mantle Sequence, whole rock pressed powder pellet boron concentrations range widely (7 to 80 µg/g, mean 34 ± 21 µg/g, n = 17; Fig. 3a). *In situ* boron concentrations from polished thick sections exhibit a similar range (3 to 49 µg/g, mean 21 ± 13 µg/g, n = 49; Fig. 3b), with notable differences between serpentine types (Fig. 3b). Mesh-textured serpentine has a higher mean boron concentration (26 ± 12 µg/g, n = 26) compared to serpentine veins (12 ± 11 µg/g, n = 20). Chrysotile veins in thick sections and pellets have boron concentrations ranging between 10 and 35 µg/g (Fig. 3).

Boron isotopic compositions ($\delta^{11}B$) of serpentine veins and serpentinites in the Troodos Mantle Sequence range from +6.7 to +18.4 ‰ (mean +11.9 ± 3.2 ‰, n = 49; Fig. 3c). Olympus and Artemis Diapirs' serpentinites have indistinguishable boron isotopic compositions, suggesting alteration by a uniform external fluid despite their different mantle origins. The Troodos Mantle Sequence's boron isotopic compositions align with those from various serpentinisation settings, yielding a mean $\delta^{11}B$ value of +17.3 ± 10.2 ‰ (n = 195; Fig. 4). Published serpentinite boron concentrations vary widely (mean $\delta^{11}B$ of 35 ± 32 µg/g, n = 195; Fig. 4b).

Discussion

High resolution (10 µm) boron elemental mapping of serpentinised mantle rocks highlights a highly heterogeneous spatial distribution of boron (Fig. 2). We interpret the three texturally distinct serpentines resulting from at least two temporally distinct alteration events. The initial pervasive serpentinisation by a fluid with a high boron concentration formed B-rich serpentine through the pseudomorphic replacement of olivine and serpentine vein precipitation. A second pervasive alteration event by a low boron concentration fluid is recorded by the mesh-textured

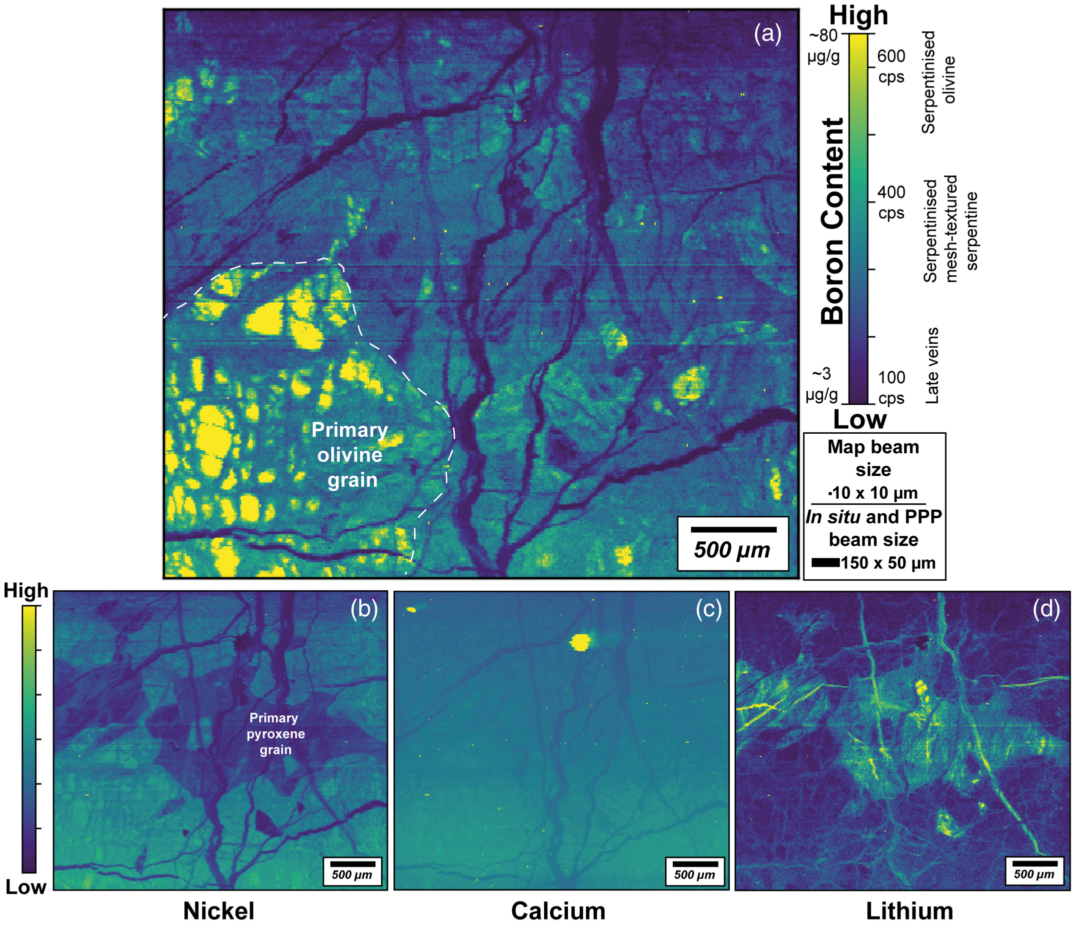

Figure 2 *In situ* **(a)** boron, **(b)** nickel, **(c)** calcium, and **(d)** lithium elemental count map of a completely serpentinised peridotite (sample AY2-2) from the Artemis Diapir. Data is plotted as counts *per* second and the relative differences are colour mapped accordingly using a linear colour map scale.

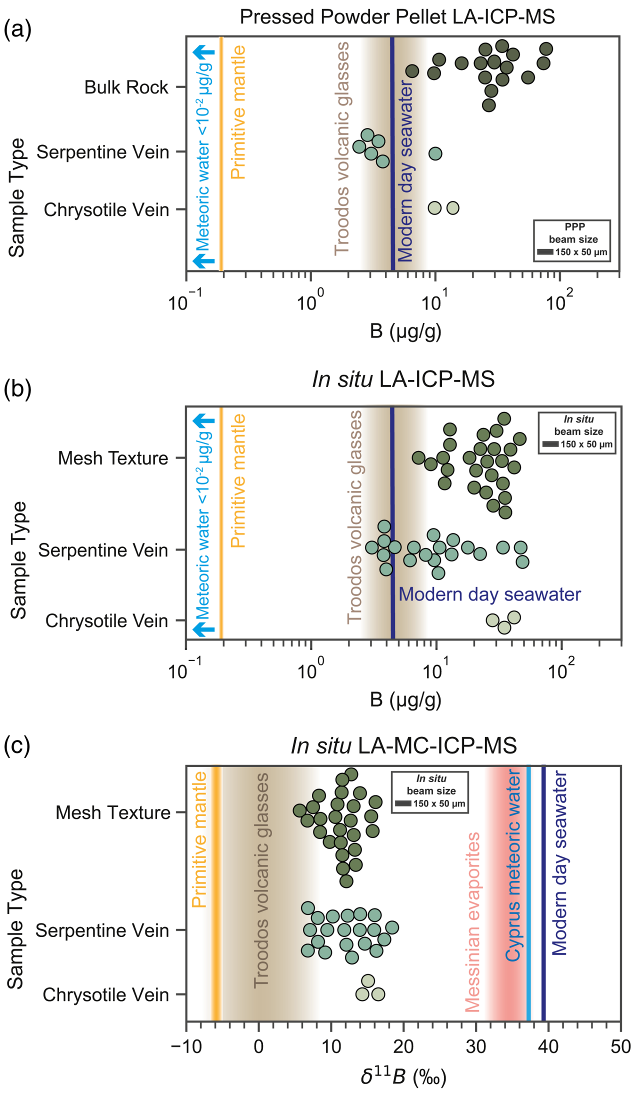

Figure 3 Caltech plots showing **(a)** B (µg/g) concentration data from pressed powder pellet LA-ICP-MS, **(b)** *In situ* LA-ICP-MS B (µg/g) concentration, **(c)** *in situ* LA-MC-ICP-MS δ^{11}B on samples from the Artemis and Olympus Diapir. Boundaries of B (µg/g) and δ^{11}B of Troodos for the reservoirs and reference materials shown are given in the Supplementary Information. Shading shows ±2σ of the reported value. Analytical errors (2 s.e.) are generally smaller than symbols.

serpentine, with lower boron concentrations indicating the differential leaching of boron. A subsequent channelled fluid event precipitated low boron and calcium but high lithium concentration serpentine in discrete veins and further leached boron from the surrounding mesh-textured host (Fig. 2).

An interpretation of multiple temporally distinct alteration events with contrasting fluid sources yielding serpentine of progressively lower boron concentrations is in agreement with the outlined geological history of the Troodos Mantle Sequence and interpretations of previous stable oxygen and hydrogen isotope analyses (Evans *et al.*, 2021). The initial high boron (~80 µg/g) pervasive serpentinisation most likely results from fluid liberated by dehydration of ocean crust and sediments from the subducting Cyprus slab (*e.g.*, Robertson, 1998; Evans *et al.*, 2021, 2024), similar to high B concentration fluids from Mariana forearc serpentinite mud volcanoes that are interpreted to be upwelling slab-derived fluids (~40 µg/g; Benton *et al.*, 2001; Mottl *et al.*, 2004).

The boron isotopic compositions (mean +11.9 ± 3.2 ‰, 1σ, n = 49) of the Olympus and Artemis diapirs are similar to strongly serpentinised ultramafic clasts recovered from Mariana forearc serpentinite mud volcanoes (mean +14.5 ± 4.5 ‰, 1σ, n = 21; Benton *et al.*, 2001). Estimating the δ^{11}B of serpentinising fluids from rock analyses is complex, requiring assumptions about the isotope partitioning of boron fluid species (Spivack and Edmond, 1987; Benton *et al.*, 2001; Boschi *et al.*, 2008; Vils *et al.*, 2009). However, at typical serpentinising conditions in the mantle wedge above subduction zones (pH > 8, ~250 °C; following McCollom *et al.* (2020), experimental determination of pK$_B$ yields values of <5 (following Dickson, 1990; Arcis *et al.*, 2017). Consequently, borate ion is the dominant fluid species resulting in minimal pH dependent fractionation (Spivack and Edmond, 1987; Benton *et al.*, 2001; Boschi *et al.*, 2008; Arcis *et al.*, 2017). The δ^{11}B of the Mariana forearc slab-derived fluid is estimated to be ~+13 ‰ (Benton *et al.*, 2001). We note that the depths of dehydration beneath the Mariana forearc (~15 to 29 km; (Mottl *et al.*, 2004) are similar to the depths of the Cyprus slab beneath the Troodos Mantle Sequence region (Feld *et al.*, 2017; Evans *et al.*, 2021). The range (+6.7 to +18.4 ‰) in δ^{11}B in Olympus and Artemis serpentinites most probably reflects the progressive evolution of a serpentinising fluid that can be modelled by Rayleigh fractionation (Eq. 1; Fig. 4a)

$$\delta^{11}B_{Fluid} = \left(\delta^{11}B_{Fluid(Initial)} + 1000\right)\left[\frac{[B_{Fluid}]}{[B_{Fluid(Initial)}]}\right]^{(\alpha-1)} - 1000$$

Eq. 1

Calculations using fractionation factors of α = 0.982 and 0.989 for 100 and 400 °C respectively (following Liu and Tossell, 2005; Boschi *et al.*, 2008) and α = 0.990 and 0.996 for 100 and 200 °C respectively (following Hansen *et al.*, 2017) indicate that as fluid boron is sequestered into serpentine the isotopic composition of the fluid evolves to higher δ^{11}B values, regardless of which fractionation factors are used (Liu and Tossell, 2005; Hansen *et al.*, 2017). Consequently, higher δ^{11}B serpentinites will precipitate further along the flow path (Spivack and Edmond, 1987; Vils *et al.*, 2009).

Hydrothermally altered seafloor lavas commonly have high boron concentrations up to 200 µg/g (Yamaoka *et al.*, 2015b; Fonseca *et al.*, 2017) and the downgoing ancient altered ocean crust of the Cyprus slab is likely a significant reservoir of boron. Consequently, we propose that dewatering and dehydration reactions during the subduction of altered ocean crust of the Cyprus slab liberated the high boron fluid responsible for the initial pervasive serpentinisation of the Troodos Mantle Sequence.

Alternative interpretations such as Cretaceous seawater-derived hydrothermal fluids penetrating through the Troodos ocean crust and into the Olympus and Artemis mantle domains do not match analyses of the Troodos ophiolite that show decreasing boron concentrations (from 207 to 0.3 µg/g) and lower δ^{11}B signatures (from +15.6 to −1.7 ‰) with depth in the ocean crust and strong channelling of hydrothermal alteration in the gabbros (Yamaoka *et al.*, 2015b). Assuming that Cretaceous seawater-derived hydrothermal fluids had similar boron isotopic compositions and concentrations to modern fluids (+13.5 to +36.1 ‰ and 4.5 to 16 µg/g respectively; Yamaoka *et al.*, 2015a), the ratio of hydrothermal fluid relative to rock required to form a high boron concentration (80 µg/g) serpentine is very high (from ~5 to ~18) and hence unlikely.

The low boron fluid end member attributed to the second and third Troodos serpentinisation events is consistent with alteration by meteoric waters, where boron derived from the initial pervasive serpentinisation is remobilised by high pH (>9) groundwaters (Evans *et al.*, 2024) leaving residual or

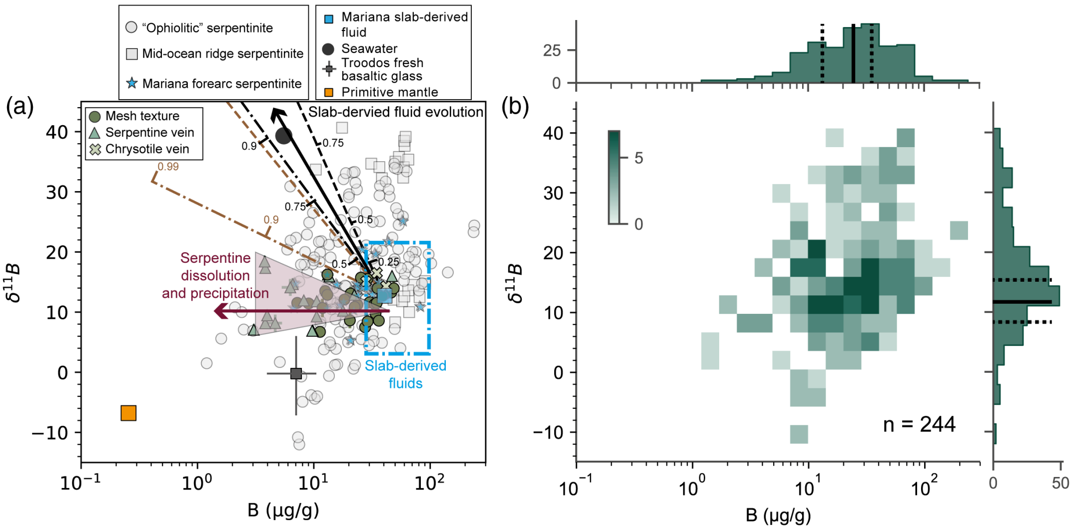

Figure 4 **(a)** δ^{11}B and B (µg/g) data from the Olympus and Artemis Diapirs of the Troodos Mantle Sequence compared with compiled published serpentinite measurements. **(b)** Density histogram plot of compiled and new δ^{11}B and B (µg/g) data. References for the compiled serpentinite values can be found in the Supplementary Information. Black solid lines of the bivariate histograms refer to the mean values of this study with dashed black lines reflecting ±1σ. Analytical error bars (2 s.e.) are shown for data from this study, most symbols are larger than associated analytical error. Simple fluid evolution model calculations using a Rayleigh fractionation model (Eq. 1) are shown as a black dashed line at 100 °C and black dash-dotted line at 400 °C using serpentine-fluid fractionation equations of Liu and Tossell (2005) and the model equations of Boschi *et al.* (2008) to estimate a fractionation factor (α). Black dash lines reflect evolution extent as B is removed from the fluid during serpentinisation at 100 and 400 °C respectively. Additionally, calculations using the serpentine-water fractionation values of Hansen *et al.* (2017) are shown as a brown dashed line at 100 °C and a brown dash-dotted line at 200 °C respectively. Initial fluid δ^{11}B and concentration of the model is set as (+13 ‰ and 40 µg/g; Benton *et al.*, 2001; Mottl *et al.*, 2004). Blue box reflects assumed composition of slab-derived fluids at similar downgoing slab depths. Purple arrow and shading show vector of serpentine dissolution and precipitation. Isotopic fractionation between mineral and fluid phases likely results in scattering of the data. Black arrow shows slab-derived fluid evolution vector.

re-precipitated serpentine with lower boron concentrations but with the boron isotope signature of the initial event (Fig. 3). This meteoric water alteration event is consistent with previous stable oxygen and hydrogen analyses (Magaritz and Taylor, 1974; Nuriel *et al.*, 2009; Evans *et al.*, 2021) and is favoured over alternative interpretations of an evolving dehydrating slab fluid source as proposed for the Mariana system (*e.g.*, Kahl *et al.*, 2015) or distinct fluid pulses with similar boron isotopic compositions but contrasting boron concentrations as suggested for the Mid-Atlantic Ridge Atlantis Massif (*e.g.*, Boschi *et al.*, 2008). These alternative interpretations are inconsistent with previous Troodos stable oxygen and hydrogen isotope compositions.

Novel high resolution elemental serpentinite mapping is a promising avenue in revealing the spatial distribution of boron and other elements (Ni, Ca, Li) in serpentinites. Elemental mapping leveraging a fine ablation beam size of 10 x 10 µm illuminates the heterogeneously distributed contrasting boron signatures that would otherwise not be observed with a coarser ablation beam or bulk rock sampling. This knowledge yields deeper interpretation of determined boron concentrations of pressed powder pellets and *in situ* polished thick sections.

In addition to boron, nickel mapping in serpentinites appears to highlight the original primary texture of mantle peridotites. Calcium mapping shows differences between mesh-textured serpentine and serpentine veins. The distributions of lithium and boron differ as these elements show contrasting affinities for serpentine that pseudomorphs olivine or pyroxene respectively. This is consistent with previous studies that demonstrate serpentine Li content is dependent on protolith mineralogy and potentially previous melt-rock interaction events (*e.g.*, Kodolányi *et al.*, 2012). The high lithium abundance in some serpentine veins within the element map (Fig. 2d) likely reflects precipitation from Li-enriched meteoric-derived hyperalkaline groundwaters (Evans *et al.*, 2024).

Future studies to identify and determine the origin of fluid in serpentinised rocks should combine elemental mapping with *in situ* measurements of oxygen and hydrogen stable isotopes as well as novel isotopic tracers such as boron to identify distinctive geochemical and isotopic fingerprints of specific serpentinisation episodes.

Acknowledgements

We thank the Geological Survey Department of the Republic of Cyprus for facilitating field work (MoU/Ref. No. 05.26.001/5). ADE acknowledges a Natural Environment Research Council-SPITFIRE CASE PhD award NE/L002531/1 (Natural History Museum CASE Partner). DAHT acknowledges a Royal Society Wolfson Research Merit Award (WM130051). We thank Prof. Raúl Fonseca for editorial handling, and Jeff Ryan and an anonymous reviewer for their constructive reviews. We thank Dan Doran and Matt Beverly-Smith for the preparation of thick sections.

Editor: Raúl Fonseca

Additional Information

Supplementary Information accompanies this letter at https://www.geochemicalperspectivesletters.org/article2407.

Cite this letter as: Evans, A.D., Standish, C.D., Milton, J.A., Robbins, A.G., Craw, D., Foster, G.L., Teagle, D.A.H. (2024) Imaging of boron in altered mantle rocks illuminates progressive serpentinisation episodes. *Geochem. Persp. Let.* 29, 20–25. https://doi.org/10.7185/geochemlet.2407

References

Alt, J.C., Shanks, W.C. (2006) Stable isotope compositions of serpentinite seamounts in the Mariana forearc: Serpentinization processes, fluid sources and sulfur metasomatism. *Earth and Planetary Science Letters* 242, 272–285. https://doi.org/10.1016/j.epsl.2005.11.063

Arcis, H., Ferguson, J.P., Applegarth, L., Zimmerman, G.H., Tremaine, P.R. (2017) Ionization of boric acid in water from 298 K to 623 K by AC conductivity and Raman spectroscopy. *The Journal of Chemical Thermodynamics* 106, 187–198. https://doi.org/10.1016/j.jct.2016.11.007

Batanova, V.G., Sobolev, A.V. (2000) Compositional heterogeneity in subduction-related mantle peridotites, Troodos massif, Cyprus. *Geology* 28, 55–58. https://doi.org/10.1130/0091-7613(2000)028<0055:CHISRM>2.3.CO;2

Benton, L.D., Ryan, J.G., Tera, F. (2001) Boron isotope systematics of slab fluids as inferred from a serpentine seamount, Mariana forearc. *Earth and Planetary Science Letters* 187, 273–282. https://doi.org/10.1016/S0012-821X(01)00286-2

Boschi, C., Dini, A., Früh-Green, G.L., Kelley, D.S. (2008) Isotopic and element exchange during serpentinization and metasomatism at the Atlantis Massif (MAR 30°N): Insights from B and Sr isotope data. *Geochimica et Cosmochimica Acta* 72, 1801–1823. https://doi.org/10.1016/j.gca.2008.01.013

Dickson, A.G. (1990) Thermodynamics of the dissociation of boric acid in synthetic seawater from 273.15 to 318.15 K. *Deep-sea Research. Part A, Oceanographic research papers* 37, 755–766. https://doi.org/10.1016/0198-0149(90)90004-F

Evans, A.D., Craw, D., Teagle, D.A.H. (2024) Active near-surface mobilisation of slab-derived geochemical signatures by hyperalkaline waters in brecciated serpentinites. *Chemical Geology* 643, 121822. https://doi.org/10.1016/j.chemgeo.2023.121822

Evans, A.D., Teagle, D.A.H., Craw, D., Henstock, T.J., Falcon-Suarez, I.H. (2021) Uplift and exposure of serpentinized massifs: Modeling differential serpentinite diapirism and exhumation of the troodos mantle sequence, Cyprus. *Journal of Geophysical Research [Solid Earth]* 126, e2020JB021079. https://doi.org/10.1029/2020JB021079

Feld, C., Mechie, J., Hübscher, C., Hall, J., Nicolaides, S., Gurbuz, C., Bauer, K., Louden, K., Weber, M. (2017) Crustal structure of the Eratosthenes Seamount, Cyprus and S. Turkey from an amphibian wide-angle seismic profile. *Tectonophysics* 700–701, 32–59. https://doi.org/10.1016/j.tecto.2017.02.003

Fonseca, R.O.C., Kirchenbaur, M., Ballhaus, C., Münker, C., Zirner, A., Gerdes, A., Heuser, A., Botcharnikov, R., Lenting, C. (2017) Fingerprinting fluid sources in Troodos ophiolite complex orbicular glasses using high spatial resolution isotope and trace element geochemistry. *Geochimica et Cosmochimica Acta* 200, 145–166. https://doi.org/10.1016/j.gca.2016.12.012

Gass, I.G., Masson-Smith, D. (1963) The Geology and Gravity Anomalies of the Troodos Massif, Cyprus. *Proceedings of the Royal Society B: Biological Sciences* 157, 587–588. https://doi.org/10.1098/rspb.1963.0030

Guillot, S., Schwartz, S., Reynard, B., Agard, P., Prigent, C. (2015) Tectonic significance of serpentinites. *Tectonophysics* 646, 1–19. https://doi.org/10.1016/j.tecto.2015.01.020

Hansen, C.T., Meixner, A., Kasemann, S.A., Bach, W. (2017) New insight on Li and B isotope fractionation during serpentinization derived from batch reaction investigations. *Geochimica et Cosmochimica Acta* 217, 51–79. https://doi.org/10.1016/j.gca.2017.08.014

Kahl, W.A., Jöns, N., Bach, W., Klein, F., Alt, J.C. (2015) Ultramafic clasts from the South Chamorro serpentine mud volcano reveal a polyphase serpentinization history of the Mariana forearc mantle. *Lithos* 227, 1–20. https://doi.org/10.1016/j.lithos.2015.03.015

Kodolányi, J., Pettke, T., Spandler, C., Kamber, B.S., Gméling, K. (2012) Geochemistry of Ocean Floor and Fore-arc Serpentinites: Constraints on the Ultramafic Input to Subduction Zones. *Journal of Petrology* 53, 235–270. https://doi.org/10.1093/petrology/egr058

Kyser, T.K., Kerrich, R. (1991) Retrograde exchange of hydrogen between hydrous minerals and water at low temperatures. In: Tayor, H.P., O'Neill, J.R., Kaplan, I.R. (Eds.) *Stable Isotope Geochemistry: a tribute to Samuel Epstein*. The Geochemical Society Special Publication, 409–422.

Liu, Y., Tossell, J.A. (2005) Ab initio molecular orbital calculations for boron isotope fractionations on boric acids and borates. *Geochimica et Cosmochimica Acta* 69, 3995–4006. https://doi.org/10.1016/j.gca.2005.04.009

Magaritz, M., Taylor Jr, H.P. (1974) Oxygen and hydrogen isotope studies of serpentinization in the Troodos ophiolite complex, Cyprus. *Earth and Planetary Science Letters* 23, 8–14. https://doi.org/10.1016/0012-821X(74)90023-5

Marschall, H.R., Wanless, V.D., Shimizu, N., Pogge von Strandmann, P.A.E., Elliott, T., Monteleone, B.D. (2017) The boron and lithium isotopic composition of mid-ocean ridge basalts and the mantle. *Geochimica Cosmochimica* 207, 102–138. https://doi.org/10.1016/j.gca.2017.03.028

Martin, C., Flores, K.E., Harlow, G.E. (2016) Boron isotopic discrimination for subduction-related serpentinites. *Geology* 44, 899–902 https://doi.org/10.1130/G38102.1

McCollom, T.M., Klein, F., Solheid, P., Moskowitz, B. (2020) The effect of pH on rates of reaction and hydrogen generation during serpentinization. *Philosophical Transactions of the Royal Society A: Mathematical, Physical and Engineering Sciences* 378, 20180428. https://doi.org/10.1098/rsta.2018.0428

Moores, E.M., Robinson, P.T., Malpas, J., Xenophonotos, C. (1984) Model for the origin of the Troodos massif, Cyprus, and other mideast ophiolites. *Geology* 12, 500–503. https://doi.org/10.1130/0091-7613(1984)12<500:MFTOOT>2.0.CO;2

Mottl, M.J., Wheat, C.G., Fryer, P., Gharib, J., Martin, J.B. (2004) Chemistry of springs across the Mariana forearc shows progressive devolatilization of the subducting plate. *Geochimica et Cosmochimica Acta* 68, 4915–4933. https://doi.org/10.1016/j.gca.2004.05.037

Nuriel, P., Katzir, Y., Abelson, M., Valley, J.W., Matthews, A., Spicuzza, M.J., Ayalon, A. (2009) Fault-related oceanic serpentinization in the Troodos ophiolite, Cyprus: Implications for a fossil oceanic core complex. *Earth and Planetary Science Letters* 282, 34–46. https://doi.org/10.1016/j.epsl.2009.02.029

Pabst, S., Zack, T., Savov, I.P., Ludwig, T., Rost, D., Vicenzi, E.P. (2011) Evidence for boron incorporation into the serpentine crystal structure. *The American Mineralogist* 96, 1112–1119. https://doi.org/10.2138/am.2011.3709

Poole, A.J., Robertson, A.H.F. (1991) Quaternary uplift and sea-level change at an active plate boundary, Cyprus. *Journal of the Geological Society of London* 148, 909–921. https://doi.org/10.1144/gsjgs.148.5.0909

Robertson, A.H.F. (1998) Mesozoic-Tertiary tectonic evolution of the easternmost Mediterranean area: integration of marine and land evidence. *Proceedings of the Ocean Drilling Program* 160, 723–782. https://doi.org/10.2973/odp.proc.sr.160.061.1998

Sheppard, S.M.F. (1980) Isotopic evidence for the origins of water during metamorphic processes in oceanic crust and ophiolite complexes. *Colloques Internationaux du CNRS* 272, 135–147.

Spivack, A.J., Edmond, J.M. (1987) Boron isotope exchange between seawater and the oceanic crust. *Geochimica et Cosmochimica Acta* 51, 1033–1043. https://doi.org/10.1016/0016-7037(87)90198-0

Vils, F., Tonarini, S., Kalt, A., Seitz, H.-M. (2009) Boron, lithium and strontium isotopes as tracers of seawater–serpentinite interaction at Mid-Atlantic ridge, ODP Leg 209. *Earth and Planetary Science Letters* 286, 414–425. https://doi.org/10.1016/j.epsl.2009.07.005

Wenner, D.B., Taylor, H.P. (1973) Oxygen and hydrogen isotope studies of the serpentinization of ultramafic rocks in oceanic environments and continental ophiolite complexes. *American Journal of Science* 273, 207–239. https://doi.org/10.2475/ajs.273.3.207

Wilson, R.A.M. (1959) *The geology of the Xeros-Troodos area*. Authority of the Government of Cyprus.

Yamaoka, K., Hong, E., Ishikawa, T., Gamo, T., Kawahata, H. (2015a) Boron isotope geochemistry of vent fluids from arc/back-arc seafloor hydrothermal systems in the western Pacific. *Chemical Geology* 392, 9–18. https://doi.org/10.1016/j.chemgeo.2014.11.009

Yamaoka, K., Matsukura, S., Ishikawa, T., Kawahata, H. (2015b) Boron isotope systematics of a fossil hydrothermal system from the Troodos ophiolite, Cyprus: Water-rock interactions in the oceanic crust and subseafloor ore deposits. *Chemical Geology 396,* 61–73. https://doi.org/10.1016/j.chemgeo.2014.12.023